



CHALMERS
UNIVERSITY OF TECHNOLOGY

Electro-assisted filtration of microfibrillated cellulose: the impact of the degree of fibrillation

Downloaded from: <https://research.chalmers.se>, 2025-03-24 14:36 UTC

Citation for the original published paper (version of record):

Hjorth, A., Vøllo Kristiansen, A., Øvrebø, H. et al (2023). Electro-assisted filtration of microfibrillated cellulose: the impact of the degree of fibrillation. *Cellulose*, 30(16): 10097-10116. <http://dx.doi.org/10.1007/s10570-023-05517-w>

N.B. When citing this work, cite the original published paper.



Electro-assisted filtration of microfibrillated cellulose: the impact of the degree of fibrillation

Anna Hjorth · Anna Vøllo Kristiansen ·
Hans Henrik Øvrebø · Hans Theliander

Received: 17 April 2023 / Accepted: 12 September 2023
© The Author(s) 2023

Abstract Efficient dewatering is necessary to achieve an economically sustainable large-scale production of microfibrillated cellulose (MFC) because the low solids content of the final product (< 3 wt.%) results in high costs related to transportation and storage, and problems for products with water incompatibility. Mechanical dewatering is preferred to thermal drying due to its lower energy demand, but MFC has a very high filtration resistance, which implies that an excessive filter area is necessary. Thus, to improve the dewatering, electro-assisted filtration may be used. In this study a bench-scale dead-end filter press was modified and the electro-assisted filtration of MFC, with two degrees of fibrillation, was investigated. The impact of the degree of fibrillation was clear when either pressure or electric field were applied

separately. It was more challenging to dewater MFC with a higher degree of fibrillation using conventional filtration due to a greater surface area being subjected to the liquid flow. The opposite was found when using an electric field alone: the more fibrillated material has a higher surface charge and thereby is impacted more by the electric field. A combination of pressure and electric field resulted in a greatly improved dewatering rate, but no significant difference could be observed between the two qualities. After dewatering, the water retention value was slightly decreased, but the material still showed a gel-like behaviour, although the network strength was slightly reduced, as seen by a reduction in yield stress, storage and loss moduli. This was plausibly due to a decrease in the surface area and/or deformed network.

Supplementary Information The online version contains supplementary material available at <https://doi.org/10.1007/s10570-023-05517-w>.

A. Hjorth · H. Theliander (✉)
Department of Chemistry and Chemical Engineering,
Chalmers University of Technology, 412 96 Gothenburg,
Sweden
e-mail: hanst@chalmers.se

A. Vøllo Kristiansen · H. H. Øvrebø
Borregaard AS, Sarpsborg, Norway

H. Theliander
Wallenberg Wood Science Center, The Royal Institute
of Technology, Chalmers University of Technology,
Linköping University, 100 44 Stockholm, Sweden

Keywords Dewatering · Electro-assisted filtration ·
Microfibrillated cellulose · Water retention value ·
Rheology

Introduction

With the increasing use of sustainable bio-based resources, such as cellulosic materials, it is important to explore and use cellulose efficiently at all length scales available: from fibre to polymeric units. Nanocelluloses, cellulose structures with dimensions in nanoscale, have attracted much attention in this context. One type of nanocellulose is fibrillated

cellulose, which can be separated from the cellulose fibre via mechanical methods (e.g. high-pressure homogenizers, microfluidizers or grinders), typically in combination with enzymatic (Pääkkö et al. 2007) or chemical pretreatment (Wågberg et al. 1987; Saito and Isogai 2004), to reduce the total energy demand. Mechanical treatment results in microfibrillated cellulose (MFC), or nanofibrillated cellulose (CNF), if the isolation of elementary fibrils is complete. The nomenclature of such fibrillated material is inconsistent in the literature so, in this paper, the distinction is made between the two types above: MFC and CNF.

MFC has received attention due to its unique properties that include a large specific surface area, a high number of hydroxyl groups exposed on the surface and a large aspect ratio. It is suggested for use in a wide range of applications such as food products (Aaen et al. 2019; Heggset et al. 2020), mechanical strength agents in paper products (Balea et al. 2020; Jele et al. 2022), barrier films (Belbekhouche et al. 2011; Lavoine et al. 2014) and paint coatings (Salo et al. 2015) to mention but a few. The list of potential future applications is nevertheless long and includes, for example, bioplastics and high-performance nanocomposites for use in optoelectronics (Hamedi et al. 2014; Hajian et al. 2017; Tian et al. 2019) and the suchlike.

The raw material and production method used affect the properties of the MFC, such as its surface charge, aspect ratio and specific surface area: this means that MFC is a diverse material rather than just one. It is therefore necessary not only to know which raw materials and process parameters result in a certain quality of MFC, but also how these influence the entire production process.

One important process parameter is the degree of fibrillation achieved by mechanical methods, because the more excessive the fibrillation, the more energy-demanding the process. This results in an MFC with a higher specific surface area and, consequently, both increased water holding capacity and bonding strength; it is important to take this into consideration when, for example, using MFC as an additive in papermaking (He et al. 2017) or in oxygen barriers and films (Siró et al. 2011; Padberg et al. 2016; Wakabayashi et al. 2020; Hasan et al. 2021).

The degree of fibrillation does not only affect the production in terms of influencing the energy

demand needed for the mechanical treatment: it also has implications for the dewatering of the resulting MFC suspension. MFC is produced in dilute suspensions (typically around 2–3 wt.% (Sinquefeld et al. 2020)) and hence water removal is necessary to facilitate economically feasible transportation, storage and/or application in various products with water incompatibility. Although water removal can be achieved through various drying techniques, these have been found to result in the partially “irreversible” aggregation of the microfibrils known as hornification (Minor 1994), which cause difficulties pertaining to re-dispersibility (Peng et al. 2012). Moreover, the excessive energy demand of thermal drying makes large-scale operation economically unfeasible.

Mechanical dewatering has the advantage of requiring less energy than thermal drying but filtration, which is the most commonly-used method for mechanical dewatering, has unfortunately proven to be challenging (Karna et al. 2021). Filtration is difficult partially because of the very large surface area of the material exposed to the liquid flow, i.e. excessive drag, and thus the high flow resistance of the filter cake being formed. Also, it has been shown that, in certain conditions, a very thin, yet dense, initial layer of particles forms on top of the filter cloth: this so-called “skin” has an resistance excessive to flow (Karna et al. 2021).

Thus, increasing the degree of fibrillation will have implications for filtration: it causes a reduction in the particle size (in this case fibril dimensions) which, in turn, leads to a higher specific surface area being subjected to the liquid flow and, consequently, more drag, i.e. higher flow resistance in the filter cake being formed. In addition, the particle size and aspect ratio may also impact the porosity of the filter cake formed, and thereby the resistance of the filter cake.

Assisted dewatering-techniques may be used to enhance the filtration of MFC: electro-assisted filtration, for example, has been shown to dewater MFC (Heiskanen et al. 2014; Karna et al. 2021) and microcrystalline cellulose (Wetterling et al. 2017a, b) successfully. Electro-assisted filtration involves an electric field being applied across a part of the filter chamber and various electrokinetic phenomena being introduced that aid the filtration, namely:

- Electrophoresis, which is the movement of charged particles relative to a surrounding fluid.

The electrophoretic velocity is proportional to the strength of the electric field and the electrophoretic movement of charged particles according to the Helmholtz-Smoluchowski Eq. (1) (Wall 2010):

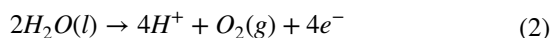
$$\frac{v_{EF}}{E} = \frac{\varepsilon\varepsilon_0\zeta}{\eta} \quad (1)$$

where v_{EF} is the electrophoretic velocity, E is the strength of the electric field applied, ε is the relative dielectric constant of the fluid, ε_0 is the permittivity of vacuum, ζ is the zeta potential and η is the dynamic viscosity of the dispersion medium.

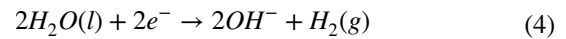
Electrophoresis may disturb the formation of a compact initial layer (i.e. a skin) of particles deposited on the filter medium and thereby affect the resistance of the filter cake. It is, however, important that the particles can migrate freely and not become locked in certain positions or hindered by, for example, an electrode or the presence of a filter cake if electrophoresis is to result in the actual migration of particles. The particles in the network nevertheless experience an electrophoretic force in the presence of an electric field.

- Electroosmotic flow of water, which results in a filtrate flow. This effect can also be described by the Helmholtz-Smoluchowski equation, although the movement of the liquid is in the opposite direction to the electrophoretic movement of the particles.
- Ohmic heating: an effect of the passage of a current through a system that has an electrical resistance. This, in turn, leads to an increase in temperature, which can be considered beneficial since it reduces the viscosity of the liquid (Weber and Stahl 2002), although too high a temperature increase may damage the material or the filter medium. In addition, ohmic heating incurs higher electrical heating costs.
- Electrolysis reactions at the electrodes (Lockhart 1983a, b; Mahmoud et al. 2010):

Anode:



Cathode:



where M is the material of the electrode and M^{n+} is its cation. Reaction [A2] dominates in the case of oxidising metals (Citeau et al. 2012).

An acidic environment is created at the anode where hydrogen ions are formed, whilst alkalinity increases at the cathode where hydroxide ions are formed. This change in pH could affect dewatering as it may alter the surface charge of the solid particles; this, in turn, depending on the pH sensibility of the solid particles, may cause their aggregation. Moreover, the presence of ionic compounds affects the conductivity of the suspension.

Electrokinetic phenomena are highly dependent on the surface charge of the solid particles in the suspension, which is affected by the degree of fibrillation. More excessive fibrillation means more surface charges are uncovered, which allows the electrokinetic phenomena to have a greater impact.

Increasing the degree of fibrillation leads to both an increased surface area and surface charge, so the question is what the outcome would be when electro-assisted filtration is employed. On the one hand, MFC with a larger surface area will experience more drag but, on the other hand, will be subjected to a greater impact of the electrokinetic phenomena because of the higher density of the surface charge. This interplay between pressure and electric field during electro-assisted filtration are examined in this study using a commercially available MFC with two different degrees of fibrillation. The experiments performed employ pressure and electric field alone, but also combine the two by using electro-assisted filtration.

In addition, there is always a risk of the partial aggregation of cellulose microfibrils during dewatering (Ding et al. 2019). It is therefore important that the dewatering process does not compromise the quality of the product, so the dewatered material is analysed in terms of water retention value (WRV) and rheological features.

Materials and methods

Material

Commercially available MFC (dry content approx. 2 wt.%) with two degrees of fibrillation were supplied by Borregaard AS, Norway.

Characterisation of the raw material

Compositional analysis

The compositional analysis was conducted according to the procedure described in Jedvert et al. (2012) that is based on the work by Theander and Westerlund (1986). In brief, 3 mL of 72% H₂SO₄ was added to a portion of 200 mg freeze-dried MFC, whereafter the sample was kept under vacuum for 15 min followed by a 30 °C water bath for 1 h. The sample was diluted with 84 g deionised water and then placed in an autoclave at 125 °C for 1 h, followed by filtration through a glass microfibre filter (Whatman GF/A). The resulting filter cake was dried at 105 °C and the amount of Klason lignin determined gravimetrically. The hydrolysate, containing monosugars and acid-soluble lignin, was quantified using HPAEC-PAD (Dionex ICS-5000) and UV/Vis spectrometry (Specord 205, Analytik Jena) at a wave length of 205 nm. Fucose (8 mg/L) was added as an internal standard in the analysis of the monosugar.

Morphology, particle size and specific surface area

Scanning electron microscopy (SEM) was used to evaluate morphology. 0.01 wt.% MFC was deposited onto a nanoporous aluminium oxide membrane (FlexiPor 20 nm, SmartMembranes GmbH), whereafter it was sputter coated (Leica EM ACE600) with a 4 nm thin layer of gold and analysed by LEO Ultra 55 SEM operating at an accelerating voltage of 3 kV.

The larger fibrils and/or fibril aggregates were analysed with kajaaniFS300 Fibre Analyzer (Metso) after dilution and dispersion. As the equipment cannot measure fibrils with a length < 0.02 mm, laser diffraction (Microtrac S3500) was used to capture the smaller fragments (detection limit: 0.02–2800 µm).

Surface charge and total charge

The surface charge of the MFC was determined using polyelectrolyte titration. MFC was diluted to 1 g/L with deionised water and titrated with poly(diallyldimethylammonium chloride) (pDAD-MAC) with a known surface charge using a Stabino Polyelectrolyte titrator (Particle Metrix GmbH, Meerbusch). The surface charge was also measured as a function of pH, in which case the pH of the suspension was adjusted with 1 M HCl or 0.5 M NaOH.

The total charge was measured by conductometric titration according to a method described by Larsson et al. (2019), whereby 0.5 g (o.d) MFC was dispersed in 80 mL of deionised water, and the pH was adjusted to 2 with 1 M HCl to protonate the sample. The volume of the sample was increased to 500 mL by the addition of deionised water, after which the solution was titrated with 0.1 M NaOH using an automatic titrator (TitroLine[®] 7000, SI analytics); the conductivity was logged continuously by means of a conductivity meter (model CO 301, VWR). The solution was purged with nitrogen throughout the titration to limit the influence of carbon dioxide.

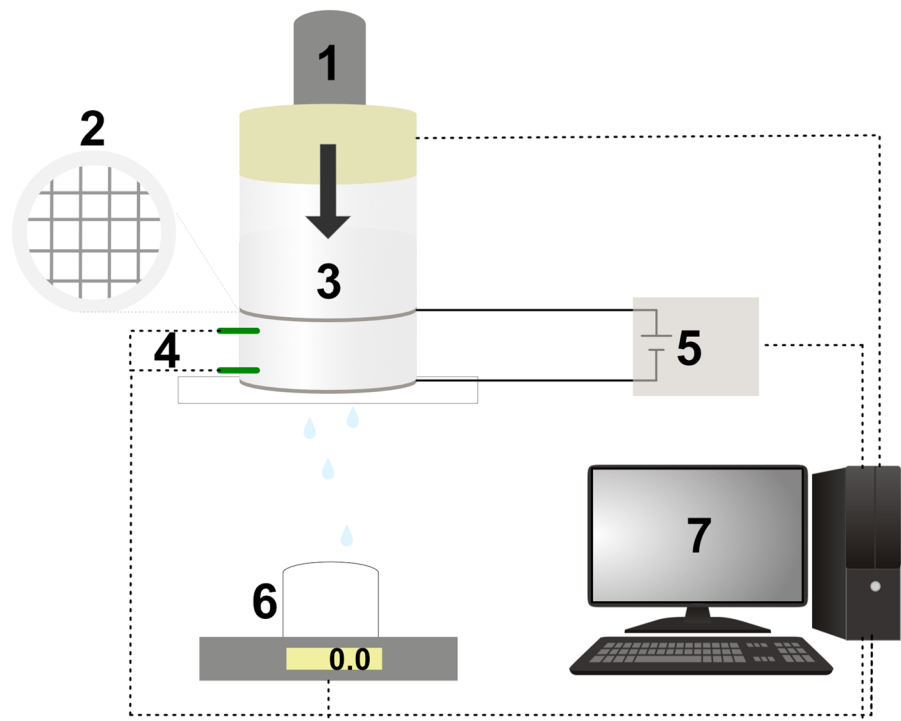
Filtration equipment

A schematic illustration of the pneumatically-driven filter press set-up used to dewater the MFC filtration is shown in Fig. 1. Further details can be found in Wetterling et al. (2017b).

The cylindrical filter cell has an inner diameter of 60 mm and total height of 175 mm, where the lower 115 mm is made out of Plexiglas. To allow for electro-assisted filtration, an electric field (DC) is applied across the lower 25 mm of the filter cell by connecting two electrodes to a power supply (EA-PSI 5200-02 A, Elektro-Automatik). The lower 30 mm of the filter cell is modified with a rack and the diameter reduced to 50 mm to accommodate an anode platinum mesh (10×10 mm, thickness 0.25 mm). The cathode, a Unimesh 300 platinum electrode, is placed on top of the bottom plate, underneath the filter support and filter medium.

Labview[™] is used to log the mass of filtrate, temperature (measured by two PFA-coated K-type thermocouples located 5 and 20 mm from the filter medium), hydrostatic pressure, power, voltage and current.

Fig. 1 Schematic illustration of the filtration set-up. (1) piston, (2) anode mesh, (3) filter cell, (4) thermocouples, (5) power supply, (6) balance and (7) data acquisition unit



The water removal was calculated according to Eq. (6):

$$\text{water removal}[\%] = 100 * \frac{m_{\text{filt}}}{m_{\text{susp}}(1 - x_{\text{MFC}})} \quad (6)$$

where m_{filt} is the amount of filtrate [g], m_{susp} the amount of suspension added to the filter cell and x_{MFC} the concentration of MFC in the suspension.

Experimental conditions

The suspension used in all filtration experiments was 1.0 wt.% MFC. It was produced the day prior to the experiment by dilution of the MFC received, followed by mechanical treatment using an IKA Ultra-Turrax® T50 with a dispersing element (S50 N-G45F) operating at 10 000 rpm for 4 min (per 300 g).

The filter medium used was a polyethersulphone membrane (PES) with a nominal pore size of 0.45 μm (Supor, PALL®), according to the manufacturer. Munktell Grade 5 filter (Ahlström-Munksjö) was used as the underlying support. All experiments were conducted at room temperature.

The effect of pressure was evaluated at three different levels: 0.3, 1.7 and 3.0 bar. Two levels of electric field were used: 16 and 32 V/cm.

The filter cakes obtained were mixed to form a homogeneous suspension, whereafter the dry content (d.c) was determined gravimetrically after drying overnight at 105 °C.

Quality analysis after filtration

Prior to quality analysis, a 2.0 wt.% suspension was prepared from the filter cake by dilution with deionised water and dispersion using IKA Ultra-Turrax® T50 with a dispersing element (S50 N-G45F) operating at 10,000 rpm for 4 min. The pH and conductivity of the sample were adjusted to 5.1 ± 0.1 and $92 \pm 9 \mu\text{S/cm}$, respectively, corresponding to that of the original suspension, using 0.05–0.5 M NaOH and 0.05–0.2 M NaCl, respectively. The sample was allowed to stabilise overnight.

Water retention value

Suspensions of 0.3 wt.% were prepared by diluting a predetermined amount of the 2.0 wt.% suspension with milliQ water, which was then disintegrated for 4 min at 8000 rpm with the IKA Ultra-Turrax® T50 with a dispersing element (S50 N-G45F). A known amount was poured into 50 mL centrifuge tubes and the suspension was left to cool before being centrifuged (5810 R, Eppendorf) for a set time at 1 000 g at room temperature (23 °C). The supernatant was discarded thereafter, and the bottom phase and centrifuge tube were weighed to calculate the WRV (g water/g MFC).

Rheology

The rheology of 0.4 wt.% suspensions were measured using a Physica MCR-301 (Anton Paar GmbH) rotational rheometer equipped with a sandblasted bob and cup. Analysis was conducted in the semi-dilute regime of 0.4 wt.%; a minimum number of duplicate measurements were performed.

A sample volume of 17 mL was transferred to the cup and allowed to equilibrate for 15 min before amplitude sweeps were performed at 1 Hz and an oscillation strain ranging from 0.01 to 100%, to determine the linear viscoelastic regime (LVE). The sample was then left to equilibrate for 15 min whereafter flow sweep measurements were performed from 0.001 to 1000 s⁻¹. After a 15-min long rest, the time sweep measurements were performed for 20 min at 1 Hz and 1% oscillation strain.

Results and discussion

Characterisation of the raw material

The compositional analysis reveals that glucose is the major component, being 97% of the monomers detected, and <3% is mannose and xylose. The lignin content is <1%.

Table 1 summarises the characterisation of the two batches of MFC: the more fibrillated material is smaller in size compared to the less fibrillated material. It is important to recognise that MFC is a

Table 1 Summary of the characterisation of the two batches of MFC using laser diffraction (Microtrac) and fibre analyser (Kajaani)

Degree of fibrillation	Low	High
Particle size d ₁₀ [µm]	6.58	6.26
Particle size d ₅₀ [µm]	34.30	20.37
Particle size d ₉₀ [µm]	137.7	64.08
L _p (length-weighted) [mm]	0.14	0.12
Width (length-weighted) [µm]	22.1	18.6

The subscripts 10, 50 and 90 indicate that x vol% of the particles are smaller than the value stated; the values correspond to averages of three replicates

polydisperse material with fibrils in many different size classes, which can be seen clearly in the micrographs in Fig. 2.

The total charge of the two batches is low: 62 ± 5 and 69 ± 4 µeq/g for the low and high degrees of fibrillation, respectively. The surface charges for the unadjusted pH (around 5.7) are reported in Table 2 and are 10.9 ± 1.2 and 13.9 ± 2.2 µeq/g for the low and high degrees of fibrillation, respectively. The surface charge is sensitive to changes in pH: Fig. 3 shows that reducing pH leads to a decrease in the surface charge due to the protonation of carboxyl groups (Fall et al. 2011). It should be noted that when pH < 3, the surface charge was too low to measure.

Dewatering microfibrillated cellulose

Dewatering 1.0 wt.% MFC suspensions was achieved via filtration (applied pressure alone), electroosmotic dewatering (applied electric field alone) and electro-assisted filtration, which is a combination of the two.

Filtration: pressure alone

Using just pressure resulted in low filtrate fluxes early on, see Fig. 4. As the particle size is larger in the less fibrillated material (cf. Table 1), it is not unexpected that the filtrate flux is slightly higher compared to the material with a higher degree of fibrillation: a smaller particle size means that a greater specific surface area is exposed to the liquid flow and there is thus more drag.

The average filtration resistance at different applied pressures was calculated through the differential form

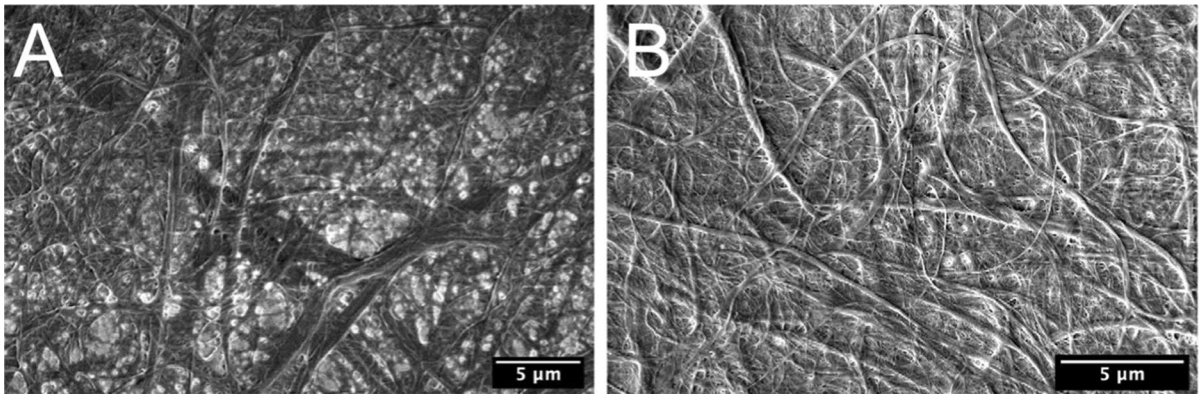


Fig. 2 Micrographs of MFC with a low (A) and high (B) degree of fibrillation

Table 2 Surface charges of the respective degrees of fibrillation at unadjusted pH

Degree of fibrillation	Low	High
Surface charge [$\mu\text{eq/g}$]	10.9 ± 1.2	13.9 ± 2.2

of the classical filtration Eq. (7) (Ruth 1935), the results of which are presented in Table 3.

$$\frac{dt}{dV} = \frac{\mu c \alpha_{av}}{A^2 \Delta P} V + \frac{\mu R_m}{A \Delta P} \quad (7)$$

Here, μ is the dynamic viscosity, c is the mass of solids per unit of filtrate volume, α_{av} is the average specific filtration resistance, A is the area of the filter cell, ΔP is the pressure drop across the filter cake and filter medium, V is the filtrate volume obtained at time t and R_m is the resistance of the filter medium. c

Fig. 3 Surface charge of MFC with a high degree of fibrillation as a function of pH

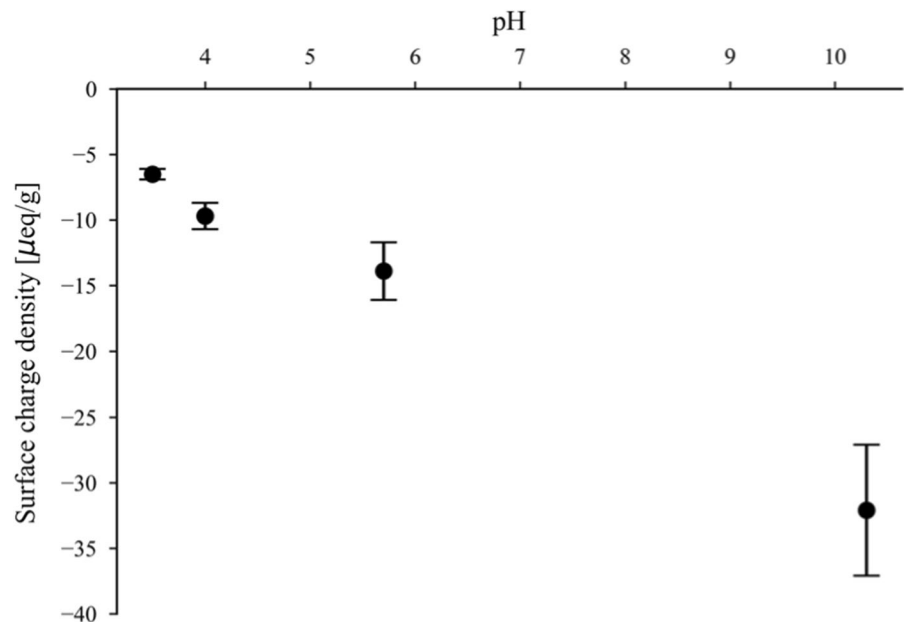


Fig. 4 Filtrate flux vs. water removal. Black line: less fibrillated material. Grey line: more fibrillated material

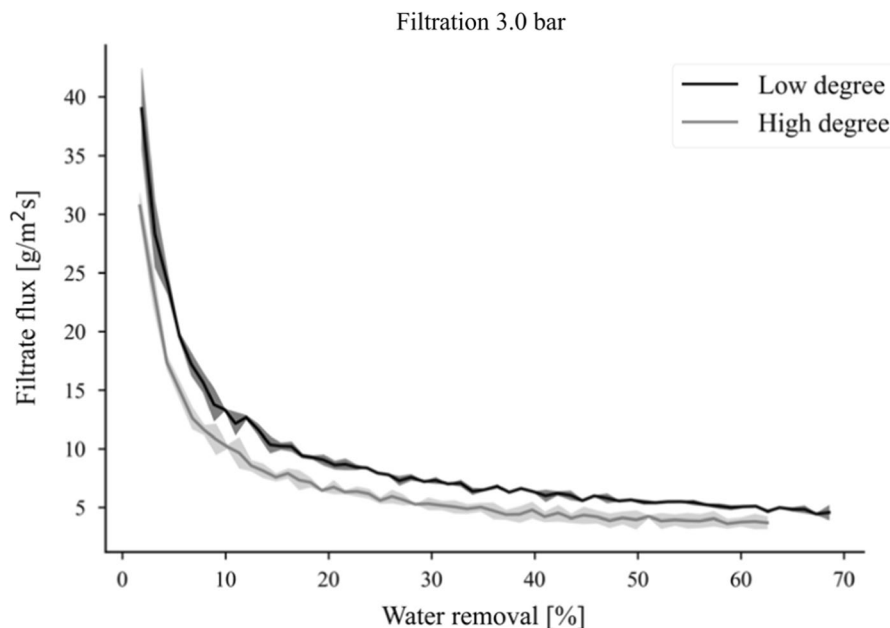


Table 3 Average filtration resistances, including standard deviations from duplicate measurements

ΔP [bar]	$\alpha_{av} * 10^{-13}$ [m/kg]	
	High degree of fibrillation	Low degree of fibrillation
0.3	0.37 ± 0.12	0.27 ± 0.01
1.7	1.96	1.12
3.0	2.95 ± 0.83	2.05 ± 0.06

No standard deviation is reported where the experiment was performed in single replicate

was calculated based on the dry mass of MFC and the total volume of filtrate collected, and was assumed to be constant.

It is important to note that Eq. (7) assumes that the filter cake is incompressible, i.e. its properties do not vary with distance from the filter medium. MFC is, on the contrary, a rather compressible material so the data presented in Table 3 should therefore be regarded as a reasonable approximation of the average filtration resistance. The table shows that the average resistances are the highest for the higher degree of fibrillation, and that the filtration resistance increases as the applied pressure increases: this behaviour is typical for compressible filter cakes (Tiller et al. 1987).

Increased pressure may lead to compaction of the particulate structure or the formation of highly resistant layers closest to the filter medium.

Increasing the applied pressure not only increases the driving force but also causes an increase in the filtration resistance and the action may thereby have an adverse effect on dewatering. This can be observed in Fig. 5, where increasing the applied pressure from 1.7 to 3.0 bar does not improve the filtrate flux when dewatering MFC with the low degree of fibrillation. The same trend is observed for the higher degree of fibrillation (see Fig. S1).

Electro-osmotic dewatering: electric field alone

The use of an electric field alone, i.e. electro-osmotic dewatering, allows the highest filtrate flux to be observed for the MFC with the highest degree of fibrillation, see Fig. 6. This concurs with expectations, since the surface charge is higher than that of the MFC with a lower degree of fibrillation (cf. Table 2). Electric field alone is insufficient to achieve much dewatering, having a degree of water removal of around 50%. In this scenario, the filter cake is not compacted to any large degree: electrophoresis makes the filter cake less dense whereas electroosmosis (to some extent) compacts it. These two opposing

Fig. 5 Filtrate flux of MFC, with a low degree of fibrillation, at the applied pressures of 0.3, 1.7 and 3.0 bar

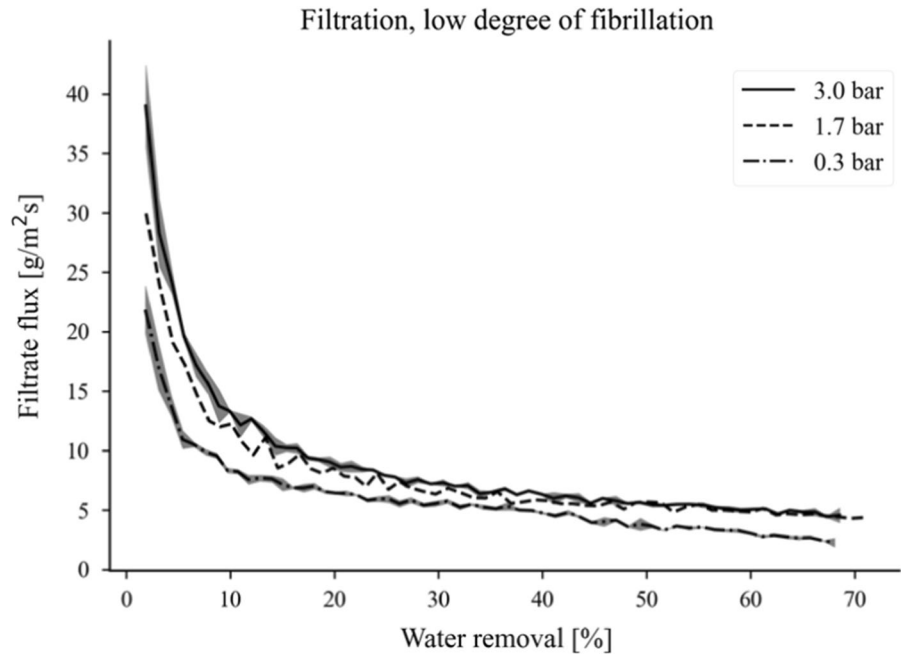
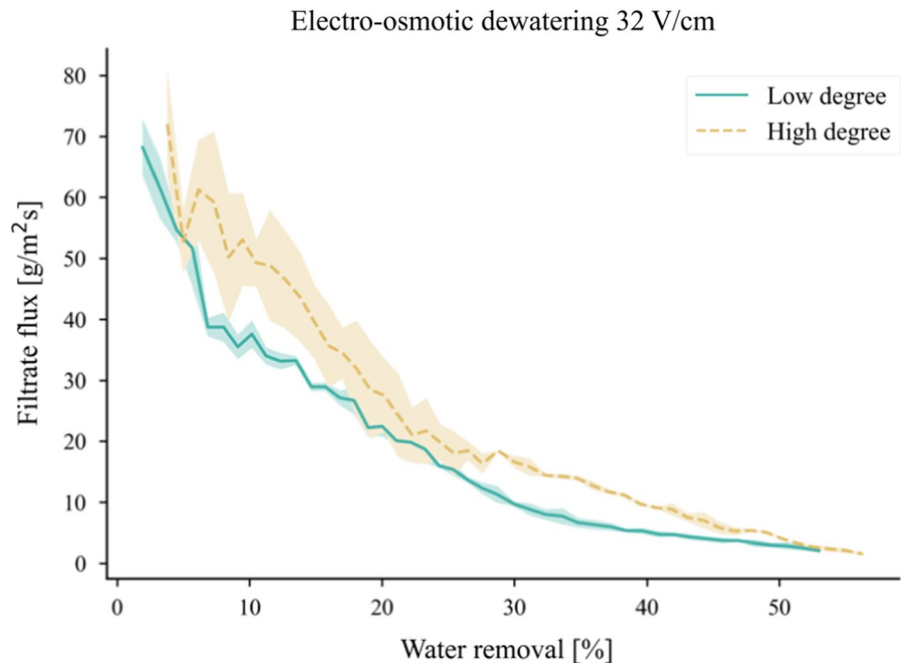


Fig. 6 Filtrate flux vs. water removal during electro-osmotic dewatering. Solid line: MFC with a low degree of fibrillation. Dashed line: MFC with a high degree of fibrillation



mechanisms do eventually reach an equilibrium that depends mainly on the properties of the solids and the electric field applied.

Electro-assisted filtration: a combination of pressure and electric field

Neither pressure nor electric field alone was sufficient in achieving effective dewatering. A combination

Fig. 7 Filtrate flux vs. water removal during electro-assisted filtration at 3.0 bar. Shaded areas indicate standard deviation. The line styles shown in the legend refer to the degree of fibrillation

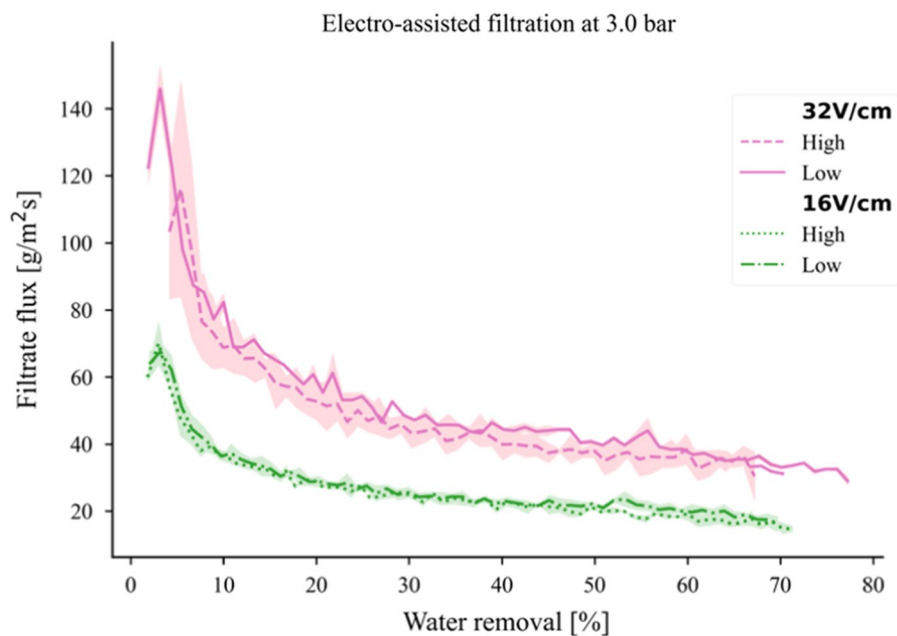
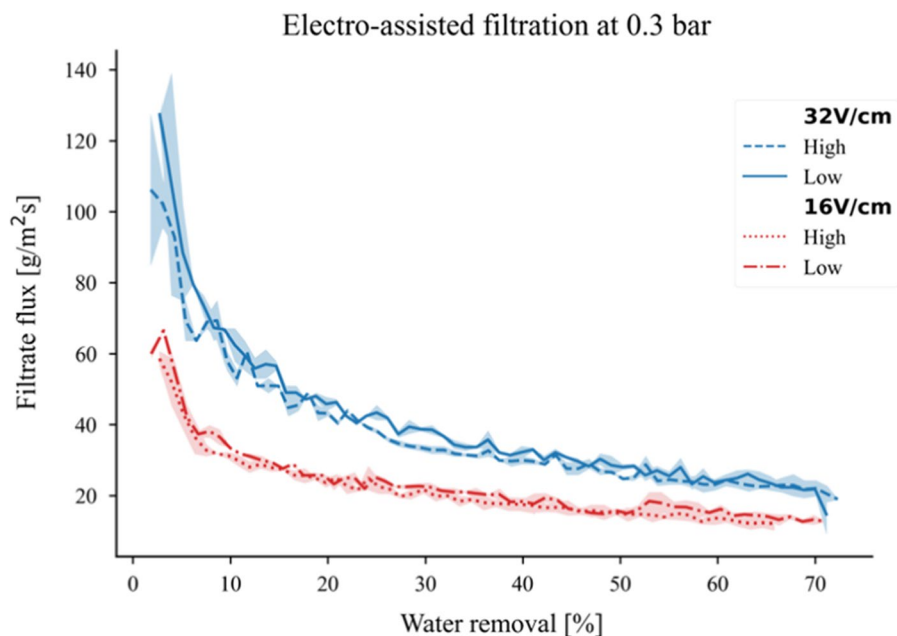


Fig. 8 Filtrate flux vs. water removal during electro-assisted filtration at 0.3 bar. Shaded areas indicate standard deviation. The line styles shown in the legend refer to the degree of fibrillation



of the two, however, yields greatly improved filtrate flux, as Figs. 7 and 8 show (see Table S1 for filtration times). Unlike earlier scenarios, where either pressure or electric field were applied separately, no significant difference can now be observed regarding the degree of fibrillation. In this case, it is the MFC with the highest degree of fibrillation that benefits the

most from using electro-assisted filtration rather than filtration.

The influence of the electric field strength is pronounced and, just as predicted by the Helmholtz-Smoluchowski Eq. (1), the highest filtrate flux is achieved with the higher electric field strength. The influence of the electrophoretic movement is greatest

in the initial phase of dewatering, when the movement of the particles is less restricted: this is what may disturb the formation of the aforementioned “skin”.

Pressure is required to press out the bulk of free water molecules (Karna et al. 2021) and some pressure is therefore essential: given the compressible nature of the material in the interval investigated, too high a pressure is however not really desirable (cf. Table 3). In the case of electro-assisted filtration, the role of electrophoresis must nevertheless be taken into consideration. It means that the effect will possibly not be the same as that observed in Table 3, where the effect of pressure during conventional filtration was examined. The filtrate flux of electro-assisted filtration at 32 V/cm and 0.3 bar (blue line) and 3.0 bar (pink line) are compared in Fig. 9. The difference is less distinct when < 10% of the water is being removed, which is where the electrophoretic movement of MFC dominates but, as dewatering proceeds, the difference becomes more pronounced. The time required to obtain a filtrate mass of 100 g only differs to a minor extent with applied pressure (see Table S1).

Images of the resulting filter cakes are shown in Fig. 10: a completely different filter cake structure is observed when electro-assisted filtration (B) is used compared to conventional filtration (A). The structure of the filter cake in the former is channelled, with

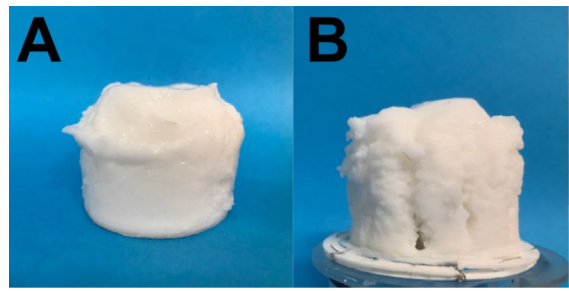
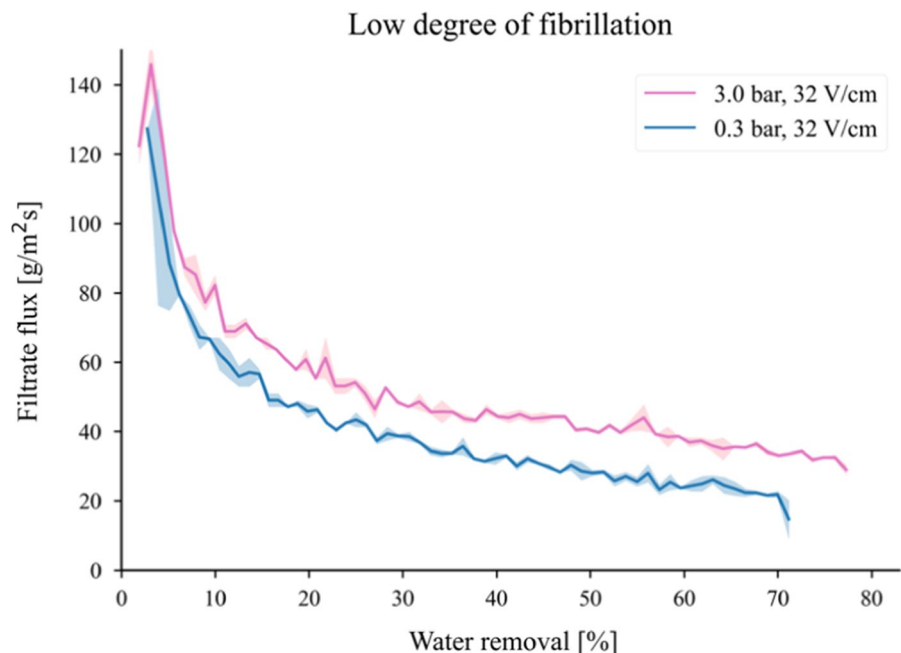


Fig. 10 Images of filter cakes after filtration with an applied pressure of 3.0 bar and filtration time of 430 min (A), and electro-assisted filtration at 3.0 bar 16 V/cm and filtration time of 140 min (B)

indications of microfibril alignment in the direction of the electric field. This alignment is not, however, as pronounced as in the case of MFC produced via 2,2,6,6-tetramethylpiperidiny-1-oxyl-mediated oxidation (TEMPO) (Lidén et al. 2022). Nevertheless, it is plausible that the somewhat channelled structure of the filter cake is one reason for its improved dewatering, as this structure has a high overall permeability.

Figure 11 presents the average dry content of the filter cakes (height 2.5 cm). The average dry content spans from 4.1 (high degree of fibrillation 0.3 bar) to 8.2% (low degree of fibrillation, 3.0 bar and 32 V/cm). It should be emphasized that the dry

Fig. 9 Filtrate flux vs. water removal during electro-assisted filtration with an applied electric field of 32 V/cm and applied pressures of 3.0 (pink line) and 0.3 bar (blue line). Material used: MFC with a low degree of fibrillation



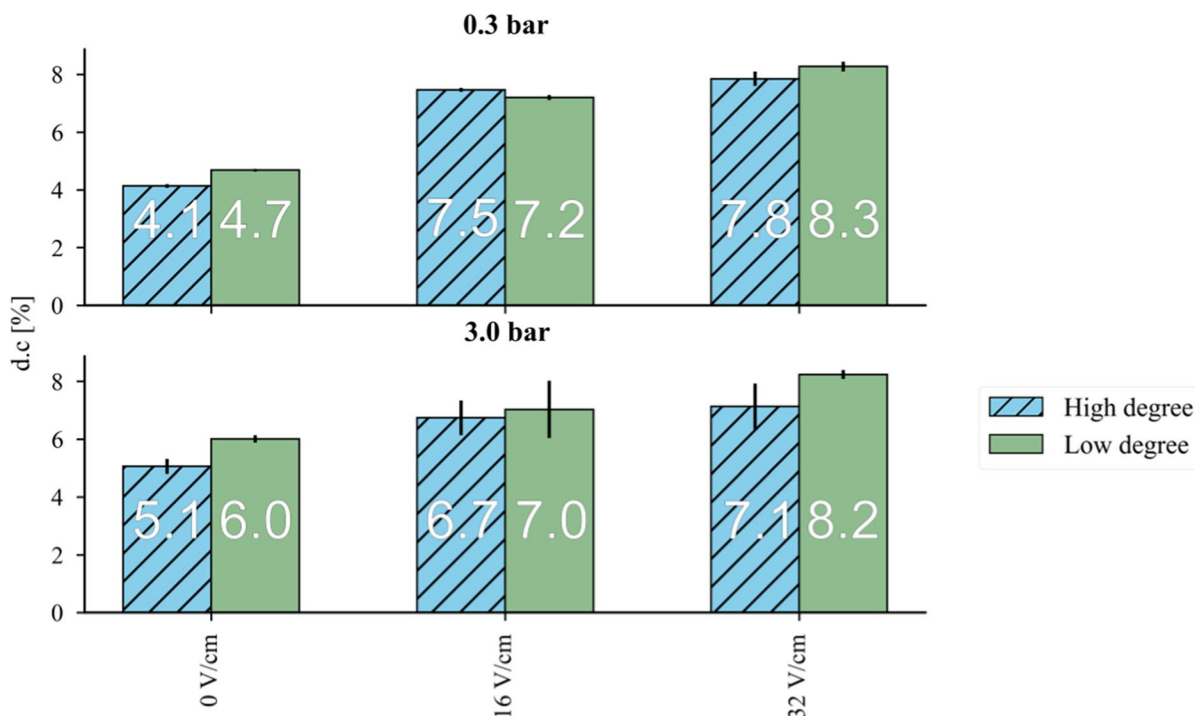


Fig. 11 Average dry content of the filter cakes. The green bars represent MFC with low degree of fibrillation and the blue hatched bars a high degree of fibrillation. The number presented on the bar refers to average dry content

content is not constant across the filter cake, but highest closest to the filter medium. The dry content could in these regions be > 10%.

Step-wise increasing the pressure

In an attempt to increase the dry content further, an incremental method was evaluated in which the pressure was increased every 15 min from 0.3 to 4.5 bar,

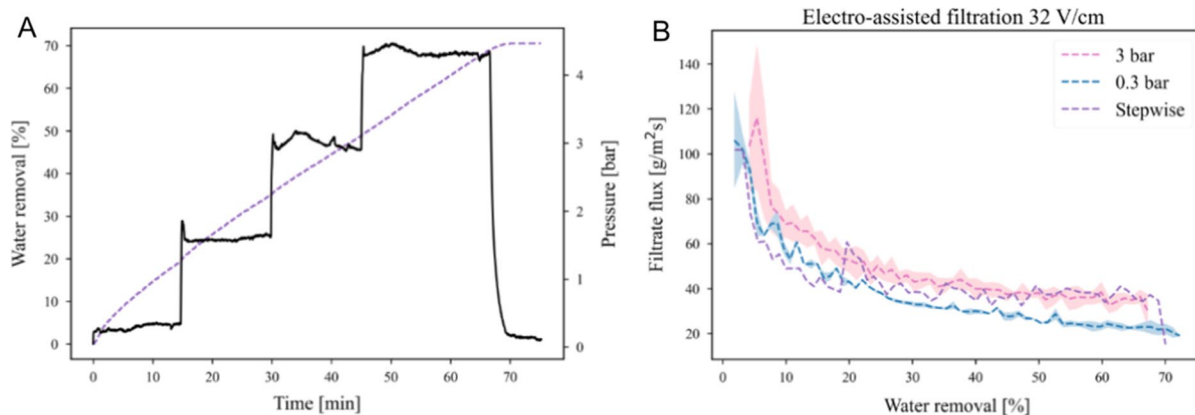


Fig. 12 **A** Water removal (purple line) and applied pressure (black line) vs. time. **B** Filtrate flux vs. water removal during electro-assisted filtration with applied electric field of 32 V/cm

cm and pressure of 3.0 bar (pink line), 0.3 bar (blue line) and increasing the pressure in increments (purple line). Material: MFC with high degree of fibrillation

see Fig. 12A. This approach was chosen because it would minimise the risk of compaction being too severe but, as can be seen in Fig. 12B, very little improvement could be detected compared to the case of constant pressure at 3.0 bar. This way of achieving a gentler compaction of the filter cake was thus found to be unsuccessful, possibly due to the influence of electrophoresis.

Effect of temperature

The temperature rises between the electrodes due to Ohmic heating, see Fig. 13. Although increasing the strength of the electric field results in an increased temperature, it did not rise more than 15 °C. Moreover, it did not cause the formation of any char, as was observed by Wetterling et al. (2018) during electro-osmotic dewatering of cellulose nanocrystals.

The temperature rise affects the liquid viscosity, see Eq. (8) (Fox et al. 2004). Raising the temperature from 20 to 35 °C reduces the viscosity of the liquid by almost 30% which, in turn, gives an increased filtrate flux.

$$\mu = 2.414 * 10^{-5} * 10^{247.8/(T-140)} \quad (8)$$

Effect of electrolysis reactions Electrolysis reactions taking place at the electrodes impact the pH and conductivity of the filter cake and filtrate, see Table 4. The pH of the filtrate is high during electro-assisted filtra-

Table 4 Summary of the pH and conductivity of the initial suspension, filtrate and filter cake (average)

	pH	Conductivity [$\mu\text{S}/\text{cm}$]
Initial suspension (1.0 wt.%)	5.2 ± 0.1	49 ± 3
<i>Filtrate</i>		
Electro-assisted filtration		
32 V/cm	10.0 ± 0.1	67 ± 6
16 V/cm	9.5 ± 0.3	61 ± 5
Filtration	6.4 ± 0.4	56 ± 4
Electro-osmotic dewatering	8.7 ± 0.5	55 ± 7
<i>Filter cake redispersed (2.0 wt.%)</i>		
Electro-assisted filtration	3.3 ± 0.1	204 ± 26
Filtration	5.1 ± 0.1	24 ± 5

tion due to the formation of hydroxide ions at the cathode. Electrolysis reactions at the cathode cause the pH of the MFC to decrease, which affects the surface charge of the material (Fig. 3). As with the dry content, the pH differs locally within the filter cake: the most acidic part is found in the vicinity of the anode.

Conductivity and pH during electro-assisted filtration were also studied (3.0 bar, 32 V/cm): samples of filtrate were collected continuously and the pH and conductivity were logged. The results, displayed in Fig. 14, show that the pH is high right from the start, indicating that the electrolysis reactions are swift. As time passes, the pH decreases, i.e. the acid front

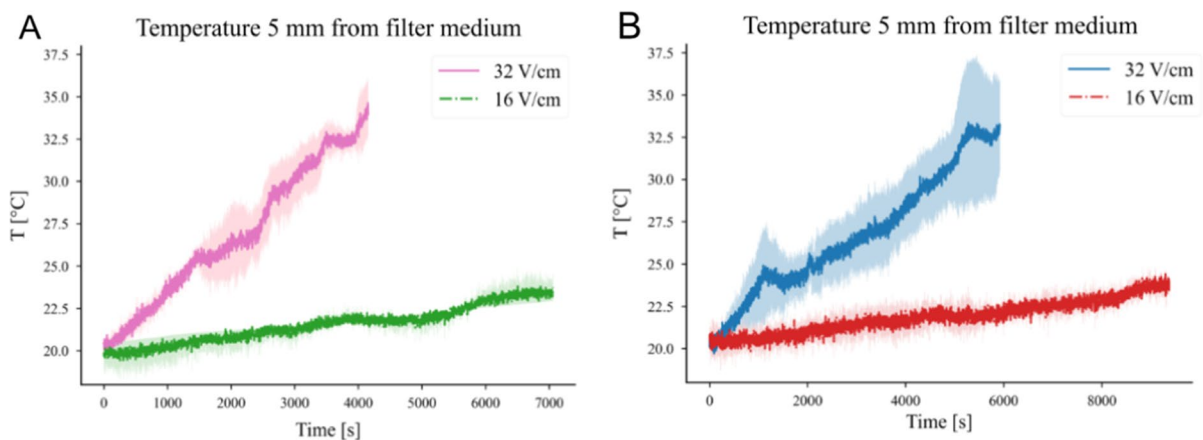


Fig. 13 Temperature profiles measured 5 mm from the filter medium with an applied pressure of 3.0 bar (A) and 0.3 bar (B). Material used: MFC with a low degree of fibrillation

Fig. 14 pH (green circles) and conductivity (blue squares) vs. cumulative mass of filtrate during electro-assisted filtration at 3.0 bar and 32 V/cm

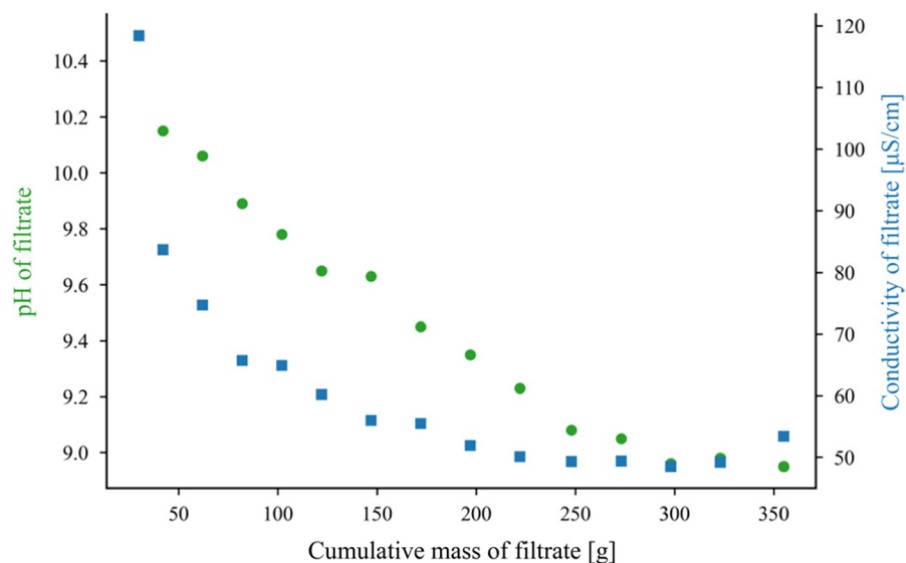
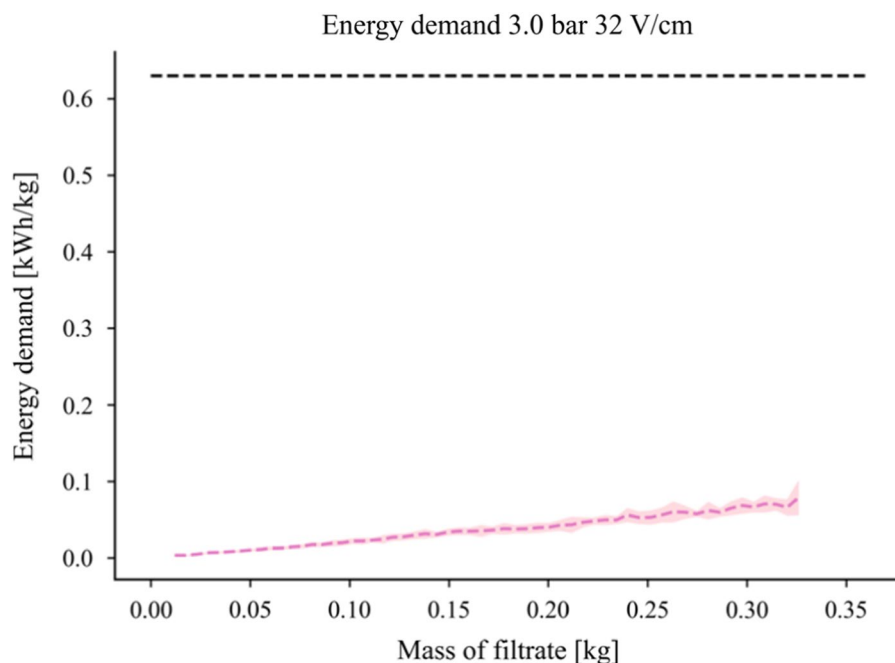


Fig. 15 Energy demand vs. mass of filtrate. Pink dashed line: electro-assisted filtration (3.0 bar 32 V/cm) of MFC with a high degree of fibrillation. Black dashed line: evaporation of water at atmospheric pressure



formed at the anode propagates through the filter cake.

Energy demand Electro-assisted filtration requires an additional energy demand but, as can be seen in Fig. 15, it is significantly less than that required for thermal drying (dashed black line) even at the higher level of applied electric field. It should be empha-

sized that the energy demand presented is for the bench-scale set-up.

The higher the electric field strength, the higher the current intensity needed to maintain a constant voltage, see Fig. 16 (Fig. S2 for applied pressure of 0.3 bar). Current intensity increases as dewatering proceeds as the concentration of MFC between

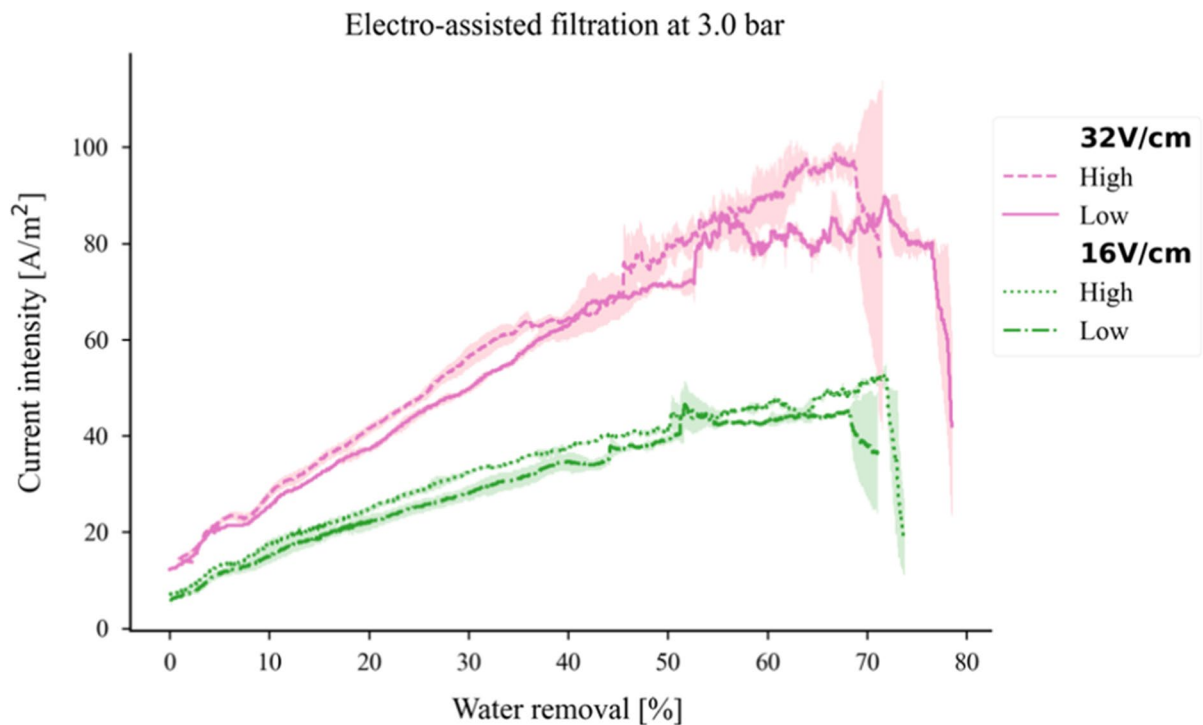


Fig. 16 Current intensity required to maintain a constant voltage vs. water removal. Shaded area: standard deviation. The line styles described in the legend refer to the degree of fibrillation

the electrodes increases and due to the formation of ionic compounds in the electrolysis reactions.

The quality of dewatered MFC

WRV

There is always a risk of hornification (the “irreversible” aggregation of microfibrils) occurring during dewatering (Ding et al. 2019) and thus a loss of WRV. The WRV measured before and after dewatering is presented in Fig. 17. It shows the same trend for both degrees of fibrillation: the WRV decreases with increasing dry content (Fig. 11). This could indicate that, after dewatering, not only is less surface area accessible but also fewer hydroxyl groups are accessible, which explains the reduced ability to hold water despite the dry contents being modest. It should be noted that, in this study, redispersion was achieved using an IKA Ultra Turrax operating at 10,000 rpm; other redispersion techniques may be available that can result in less of a reduction.

Rheology

MFC displays a classical shear thinning flow profile before and after dewatering (Fig. 18). This behaviour has been reported recurrently in the literature (e.g. Agoda-Tandjawa et al. 2010; Iotti et al. 2011; Cinar Ciftci et al. 2020) and is attributed to the structuring and alignment of MFC in the direction of the shear, which thereby decreases the viscosity at high shear rates (Hubbe et al. 2017).

The yield stress was determined from the amplitude sweep profile from a 10% decline of the storage modulus from the plateau value of the LVE region (Mezger 2020) (see Fig. S3) and is tabulated in Table 5. The values should be evaluated in relative means rather than absolute numbers, as there are many different ways of determining yield stress. The dewatered materials display slightly more delicate gels with lower yield stress, i.e. less force is needed to deform the elastic structure after dewatering and redispersion.

The equilibrium moduli after 20 min determined from time sweep measurements in the LVE-region are

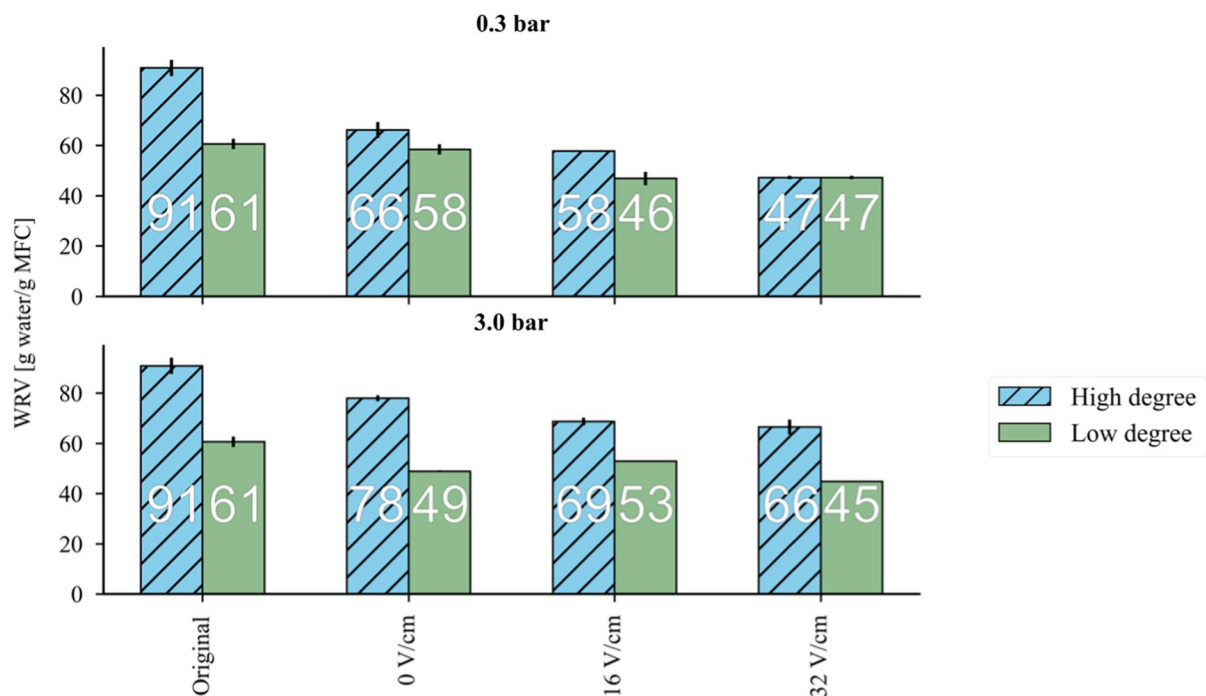


Fig. 17 WRV, including standard deviation. Upper bars: applied pressure of 0.3 bar. Lower bars: applied pressure of 3.0 bar. The number on each bar refers to the average WRV

Fig. 18 Flow sweep profile of 0.4 wt.% MFC with a low degree of fibrillation, presented as average values of three separate replicates

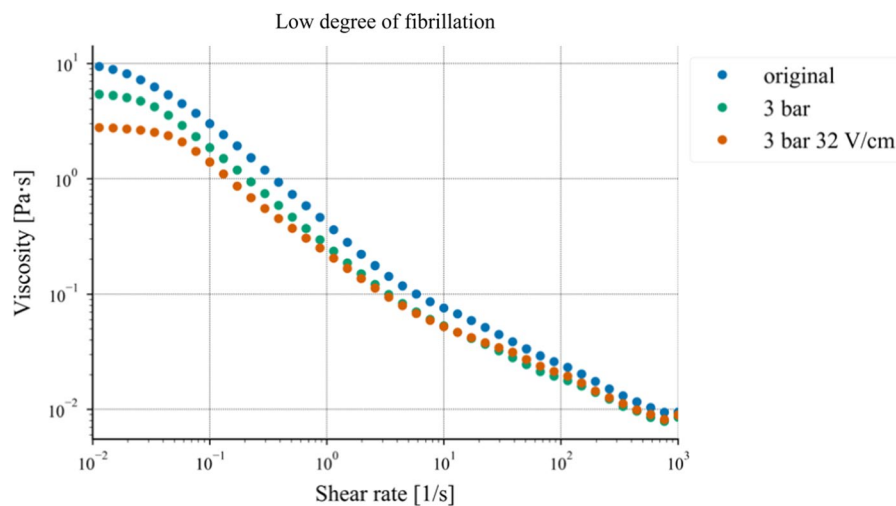


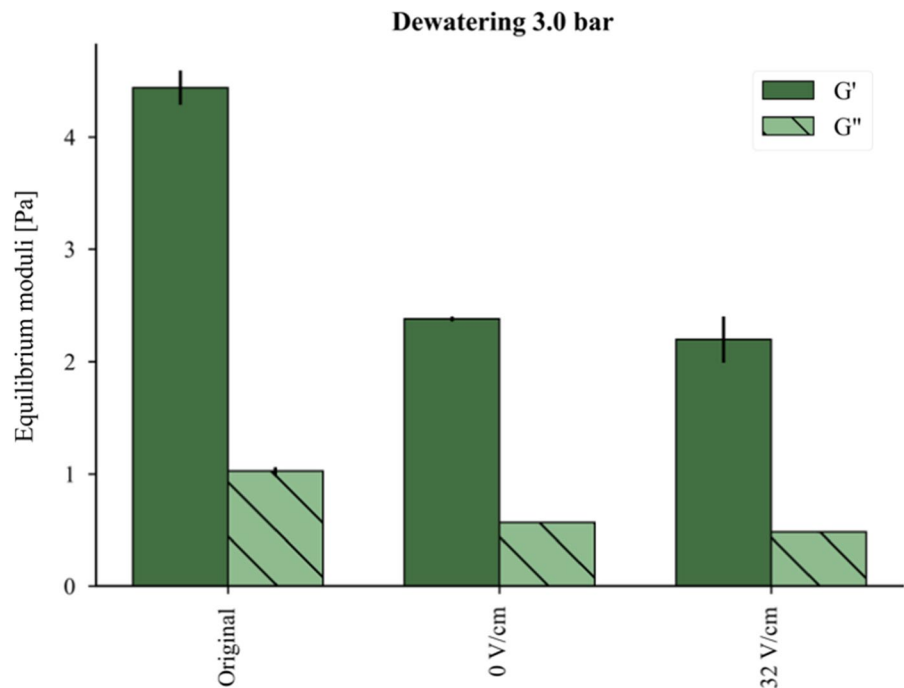
Table 5 Yield stress of MFC with a low degree of fibrillation, including standard deviation from triplicate measurements

	Original	3.0 bar	3.0 bar 32 V/cm
Yield stress [Pa]	0.079 ± 0.005	0.054 ± 0.001	0.046 ± 0.002

All suspensions were analysed at a concentration of 0.4 wt.%

presented in Fig. 19: the 0.4 wt.% MFC exhibits a gel-like viscoelastic behaviour because the elastic modulus (G') is larger than the loss modulus (G'') for all samples analysed. The values of G' and G'' do, however, decrease as the dry content increases (Fig. 11). This reduction may, once again, be an indication of less surface area being accessible after dewatering. A

Fig. 19 Equilibrium moduli, including standard deviation from duplicate measurements, for MFC with a low degree of fibrillation (0.4 wt.%)



decrease in the amount of surface area available could mean fewer contact points for the fibrils and, consequently, a weaker fibril network.

Final remarks on quality after dewatering

Both the WRV and rheology measurements indicate that the microfibril network is weaker after dewatering. The full reason behind this is not understood as yet, but one plausible reason is related to the partial aggregation or reshaping of the microfibrils/fibril bundles, which makes redispersion more difficult (even though no visible aggregates could be detected). This, in turn, could mean less surface area is available and therefore there are fewer contact points, or the network is deformed and its strength is thereby reduced.

A fibril network that is reduced in strength could have implications for the final usage of the product. It should, however, be recognised that if MFC is to be used in combination with another material, e.g. in a bio composite, this additional ingredient could also affect the rheological properties of the final product. On the other hand, there are alternative avenues that can be explored if a reduction in network strength is not allowed: Cinar Ciftci et al. (2020), for example, showed that the rheological features could be tailored

by mixing MFC of different size fractions. Also, the chemical environment could be finetuned (Fall et al. 2022), but this lies beyond the scope of the present study.

Conclusions

This study has evaluated the dewatering of commercially available MFC with two degrees of fibrillation using pressure and electric field. Filtration of the MFC was challenging and the resulting filter cakes were compressible in nature; the average filtration resistance increased with increasing applied pressure, in the pressure range evaluated. The impact of the degree of fibrillation was clear when the effect of pressure alone was evaluated, and the dewatering rate decreased with increasing degree of fibrillation. This is related to the increasing total surface area of the material subjected to the liquid flow, causing more drag. When an electric field alone was applied, the opposite was true: the more fibrillated material had a higher dewatering rate. This was due to a higher surface charge, resulting in the electric field having a greater impact.

When a combination of pressure and electric field was used, i.e. electro-assisted filtration, the

dewatering improved significantly; moreover, it required less energy than thermal drying. The effect of electro-assisted filtration was greater for the higher degree of fibrillation compared to filtration, although no significant differences were observed between the two degrees of fibrillation investigated.

After dewatering, the WRV and rheology of a redispersed suspension (10 000 rpm) were assessed. The WRV decreased after dewatering, with the decreasing trend appearing to be slightly related to an increasing dry content of the filter cake. The MFC still showed gel-like behaviour ($G' > G''$) after dewatering using filtration and electro-assisted filtration, albeit that a reduction in the yield stress and equilibrium moduli (G' and G'') indicated a weakening of the network strength. It is plausible that this is due to the partial aggregation and/or reshaping of the microfibrils/fibril bundles.

Acknowledgments The financial support received from The Swedish Research Council (Vetenskapsrådet) is gratefully acknowledged. The SEM analysis was performed at the Chalmers Material Analysis Laboratory, CMAL, in Gothenburg. Ph.D. student Farhiya Sellman at The Royal Institute of Technology, Stockholm, is thanked for performing the surface charge analysis and Dr. Anders Åkesjö for the 3D printing material. Also, Ms. Anne Opstad and Ms. Anne Marie Falkenberg Olsen at Borregaard are thanked for their kind assistance.

Author contributions All authors contributed to the study conception and design. Experimental work was performed by AH. The first draft of the manuscript was written by AH and all authors commented on previous versions of the manuscript. All authors read and approved the final manuscript.

Funding Open access funding provided by Chalmers University of Technology. This work was supported by the Swedish Research Council (Vetenskapsrådet) (Grant number 2017-04521). The authors have received research support from Chalmers Material Analysis Laboratory and Borregaard AS.

Data availability Not applicable.

Declarations

Conflict of interest All the authors declare no conflicts of interest.

Consent to participate Not applicable.

Consent for publication All authors have given their consent to submit.

Open Access This article is licensed under a Creative Commons Attribution 4.0 International License, which permits

use, sharing, adaptation, distribution and reproduction in any medium or format, as long as you give appropriate credit to the original author(s) and the source, provide a link to the Creative Commons licence, and indicate if changes were made. The images or other third party material in this article are included in the article's Creative Commons licence, unless indicated otherwise in a credit line to the material. If material is not included in the article's Creative Commons licence and your intended use is not permitted by statutory regulation or exceeds the permitted use, you will need to obtain permission directly from the copyright holder. To view a copy of this licence, visit <http://creativecommons.org/licenses/by/4.0/>.

References

- Aaen R, Simon S, Wernersson Brodin F, Syverud K (2019) The potential of TEMPO-oxidized cellulose nanofibrils as rheology modifiers in food systems. *Cellulose* 26:5483–5496. <https://doi.org/10.1007/s10570-019-02448-3>
- Agoda-Tandjawa G, Durand S, Berot S et al (2010) Rheological characterization of microfibrillated cellulose suspensions after freezing. *Carbohydr Polym* 80:677–686. <https://doi.org/10.1016/j.carbpol.2009.11.045>
- Balea A, Fuente E, Monte MC et al (2020) Industrial application of nanocelluloses in papermaking: a review of challenges, technical solutions, and market perspectives. *Molecules* 25:526. <https://doi.org/10.3390/molecules25030526>
- Belbekhouche S, Bras J, Siqueira G et al (2011) Water sorption behavior and gas barrier properties of cellulose whiskers and microfibrils films. *Carbohydr Polym* 83:1740–1748. <https://doi.org/10.1016/j.carbpol.2010.10.036>
- Cinar Ciftci G, Larsson PA, Riazanova AV et al (2020) Tailoring of rheological properties and structural polydispersity effects in microfibrillated cellulose suspensions. *Cellulose* 27:9227–9241. <https://doi.org/10.1007/s10570-020-03438-6>
- Citeau M, Larue O, Vorobiev E (2012) Influence of filter cell configuration and process parameters on the electro-osmotic dewatering of sewage sludge. *Sep Sci Technol* 47:11–21. <https://doi.org/10.1080/01496395.2011.616567>
- Ding Q, Zeng J, Wang B et al (2019) Effect of nanocellulose fiber hornification on water fraction characteristics and hydroxyl accessibility during dehydration. *Carbohydr Polym* 207:44–51. <https://doi.org/10.1016/j.carbpol.2018.11.075>
- Fall AB, Lindström SB, Sundman O et al (2011) Colloidal stability of aqueous nanofibrillated cellulose dispersions. *Langmuir* 27:11332–11338. <https://doi.org/10.1021/la201947x>
- Fall A, Henriksson M, Karppinen A et al (2022) The effect of ionic strength and pH on the dewatering rate of cellulose nanofibril dispersions. *Cellulose* 29:7649–7662. <https://doi.org/10.1007/s10570-022-04719-y>
- Fox RW, McDonald AT, Pritchard PJ (2004) Introduction to fluid mechanics, 6th edn. Wiley, New York
- Hajian A, Lindström SB, Pettersson T et al (2017) Understanding the dispersive action of nanocellulose for carbon

- nanomaterials. *Nano Lett* 17:1439–1447. <https://doi.org/10.1021/acs.nanolett.6b04405>
- Hamed MM, Hajian A, Fall AB et al (2014) Highly conducting, strong nanocomposites based on nanocellulose-assisted aqueous dispersions of single-wall carbon nanotubes. *ACS Nano* 8:2467–2476. <https://doi.org/10.1021/nn4060368>
- Hasan I, Wang J, Tajvidi M (2021) Tuning physical, mechanical and barrier properties of cellulose nanofibril films through film drying techniques coupled with thermal compression. *Cellulose* 28:11345–11366. <https://doi.org/10.1007/s10570-021-04269-9>
- He M, Yang G, Cho B-U et al (2017) Effects of addition method and fibrillation degree of cellulose nanofibrils on furnish drainability and paper properties. *Cellulose* 24:5657–5669. <https://doi.org/10.1007/s10570-017-1495-3>
- Heggset EB, Aaen R, Veslum T et al (2020) Cellulose nanofibrils as rheology modifier in mayonnaise—a pilot scale demonstration. *Food Hydrocolloids* 108:106084. <https://doi.org/10.1016/j.foodhyd.2020.106084>
- Heiskanen I, Backfolk K, Kotilainen A, et al (2014) Process for treating microfibrillated cellulose and microfibrillated cellulose treated according to the process
- Hubbe MA, Tayeb P, Joyce M et al (2017) Rheology of nanocellulose-rich aqueous suspensions: a review. *Biores* 12:9556–9661. <https://doi.org/10.15376/biores.12.4.Hubbe>
- Iotti M, Gregersen ØW, Moe S, Lenes M (2011) Rheological studies of microfibrillar cellulose water dispersions. *J Polym Environ* 19:137–145. <https://doi.org/10.1007/s10924-010-0248-2>
- Jedvert K, Saltberg A, Theliander H et al (2012) BIOREFINERY: mild steam explosion: a way to activate wood for enzymatic treatment, chemical pulping and biorefinery processes. *Nord Pulp Pap Res J* 27:828–835. <https://doi.org/10.3183/npprj-2012-27-05-p828-835>
- Jele TB, Lekha P, Sithole B (2022) Role of cellulose nanofibrils in improving the strength properties of paper: a review. *Cellulose* 29:55–81. <https://doi.org/10.1007/s10570-021-04294-8>
- Karna NK, Lidén A, Wohlert J, Theliander H (2021) Electroassisted filtration of microfibrillated cellulose: insights gained from experimental and simulation studies. *Ind Eng Chem Res*. <https://doi.org/10.1021/acs.iecr.1c03749>
- Larsson PA, Riazanova AV, Cinar Ciftci G et al (2019) Towards optimised size distribution in commercial microfibrillated cellulose: a fractionation approach. *Cellulose* 26:1565–1575. <https://doi.org/10.1007/s10570-018-2214-4>
- Lavoine N, Desloes I, Khelifi B, Bras J (2014) Impact of different coating processes of microfibrillated cellulose on the mechanical and barrier properties of paper. *J Mater Sci* 49:2879–2893. <https://doi.org/10.1007/s10853-013-7995-0>
- Lidén A, Naidjonoka P, Karna NK, Theliander H (2022) Structure of filter cakes during the electroassisted filtration of microfibrillated cellulose. *Ind Eng Chem Res* 61:16247–16256. <https://doi.org/10.1021/acs.iecr.2c03216>
- Lockhart NC (1983a) Electroosmotic dewatering of clays. I. Influence of voltage. *Colloids Surf* 6:229–238. [https://doi.org/10.1016/0166-6622\(83\)80015-8](https://doi.org/10.1016/0166-6622(83)80015-8)
- Lockhart NC (1983b) Electroosmotic dewatering of clays. II. Influence of salt, acid and flocculants. *Colloids Surf* 6:239–251. [https://doi.org/10.1016/0166-6622\(83\)80016-X](https://doi.org/10.1016/0166-6622(83)80016-X)
- Mahmoud A, Olivier J, Vaxelaire J, Hoadley AFA (2010) Electrical field: a historical review of its application and contributions in wastewater sludge dewatering. *Water Res* 44:2381–2407. <https://doi.org/10.1016/j.watres.2010.01.033>
- Mezger T (2020) 8. Oscillatory tests. *The rheology handbook: for users of rotational and oscillatory rheometers*. Vincentz Network, Hanover, pp 153–247
- Minor JL (1994) Hornification-its origin and meaning. *Prog Pap Recycl* 3:93–95
- Pääkkö M, Ankerfors M, Kosonen H et al (2007) Enzymatic hydrolysis combined with mechanical shearing and high-pressure homogenization for nanoscale cellulose fibrils and strong gels. *Biomacromol* 8:1934–1941. <https://doi.org/10.1021/bm061215p>
- Padberg J, Gliese T, Bauer W (2016) The influence of fibrillation on the oxygen barrier properties of films from microfibrillated cellulose. *Nord Pulp Pap Res J* 31:548–560. <https://doi.org/10.3183/npprj-2016-31-04-p548-560>
- Peng Y, Gardner DJ, Han Y (2012) Drying cellulose nanofibrils: in search of a suitable method. *Cellulose* 19:91–102. <https://doi.org/10.1007/s10570-011-9630-z>
- Ruth BF (1935) Studies in filtration III. derivation of general filtration equations. *Ind Eng Chem* 27:708–723. <https://doi.org/10.1021/ie50306a024>
- Saito T, Isogai A (2004) TEMPO-mediated oxidation of native cellulose. The effect of oxidation conditions on chemical and crystal structures of the water-insoluble fractions. *Biomacromol* 5:1983–1989. <https://doi.org/10.1021/bm0497769>
- Salo T, Dimic-Misic K, Gane P, Paltakari J (2015) Application of pigmented coating colours containing MFC/NFC: Coating properties and link to rheology. *Nord Pulp Pap Res J* 30:165–178. <https://doi.org/10.3183/npprj-2015-30-01-p165-178>
- Sinquefield S, Ciesielski PN, Li K et al (2020) Nanocellulose dewatering and drying: current state and future perspectives. *ACS Sustainable Chem Eng* 8:9601–9615. <https://doi.org/10.1021/acssuschemeng.0c01797>
- Siró I, Plackett D, Hedenqvist M et al (2011) Highly transparent films from carboxymethylated microfibrillated cellulose: the effect of multiple homogenization steps on key properties. *J Appl Polym Sci* 119:2652–2660. <https://doi.org/10.1002/app.32831>
- Theander O, Westerlund EA (1986) Studies on dietary fiber. 3. Improved procedures for analysis of dietary fiber. *J Agric Food Chem* 34:330–336. <https://doi.org/10.1021/jf00068a045>
- Tian W, Vahid MA, Reid MS et al (2019) Multifunctional nanocomposites with high strength and capacitance using 2D MXene and 1D nanocellulose. *Adv Mater* 31:1902977. <https://doi.org/10.1002/adma.201902977>
- Tiller FM, Yeh CS, Leu WF (1987) Compressibility of particulate structures in relation to thickening, filtration, and expression—a review. *Sep Sci Technol* 22:1037–1063. <https://doi.org/10.1080/01496398708068998>

- Wågberg L, Winter L, Ödberg L, Lindström T (1987) On the charge stoichiometry upon adsorption of a cationic polyelectrolyte on cellulosic materials. *Colloids Surf* 27:163–173. [https://doi.org/10.1016/0166-6622\(87\)80335-9](https://doi.org/10.1016/0166-6622(87)80335-9)
- Wakabayashi M, Fujisawa S, Saito T, Isogai A (2020) Nanocellulose film properties tunable by controlling degree of fibrillation of TEMPO-oxidized cellulose. *Front Chem* 8:37
- Wall S (2010) The history of electrokinetic phenomena. *Curr Opin Colloid Interface Sci* 15:119–124. <https://doi.org/10.1016/j.cocis.2009.12.005>
- Weber K, Stahl W (2002) Improvement of filtration kinetics by pressure electrofiltration. *Sep Purif Technol* 26:69–80. [https://doi.org/10.1016/S1383-5866\(01\)00118-6](https://doi.org/10.1016/S1383-5866(01)00118-6)
- Wetterling J, Jonsson S, Mattsson T, Theliander H (2017a) The influence of ionic strength on the electroassisted filtration of microcrystalline cellulose. *Ind Eng Chem Res* 56:12789–12798. <https://doi.org/10.1021/acs.iecr.7b03575>
- Wetterling J, Mattsson T, Theliander H (2017b) Local filtration properties of microcrystalline cellulose: influence of an electric field. *Chem Eng Sci* 171:368–378. <https://doi.org/10.1016/j.ces.2017.05.054>
- Wetterling J, Sahlin K, Mattsson T et al (2018) Electroosmotic dewatering of cellulose nanocrystals. *Cellulose* 25:2321–2329. <https://doi.org/10.1007/s10570-018-1733-3>

Publisher's Note Springer Nature remains neutral with regard to jurisdictional claims in published maps and institutional affiliations.